J Mater Sci (2006) 41:7798–7807
DOI 10.1007/s10853-006-0728-x

Interface structure and strain development during compression tests of Al_2O_3/Nb/Al_2O_3 sandwiches

C. Scheu · Y. Liu · S. H. Oh · D. Brunner · M. Rühle

Received: 23 April 2006 / Accepted: 28 July 2006 / Published online: 24 October 2006

Abstract The interface structure of an Al_2O_3/Nb/Al_2O_3 sandwich produced by solid-state diffusion bonding was investigated in detail by various transmission electron microscopy (TEM) methods. The joint possessed at one interface a $(110)_{Nb} \parallel (0001)_{Al_2O_3}$, $[1\bar{1}0]_{Nb} \parallel [2\bar{1}\bar{1}0]_{Al_2O_3}$, and on the other interface a $(110)_{Nb} \parallel (0001)_{Al_2O_3}$ and $[1\bar{1}0]_{Nb} \parallel [0\bar{1}\bar{1}0]_{Al_2O_3}$ orientation relationship. At both interfaces, misfit dislocations formed to compensate the lattice mismatch as found by high-resolution transmission electron microscopy (HRTEM). Electron energy-loss near edge structure (ELNES) studies revealed that the interface is terminating with an Al layer resulting in Al–Nb bonds. Identical sandwiches were investigated on the meso- and macroscopic scale by performing compression tests and simultaneously monitoring the strain development at $(001)_{Nb}$ and $(1\bar{1}0)_{Nb}$ crystal faces. The full-field optical strain measurements (FFOM) revealed that the strain is localized at the interfaces when observed at the $(001)_{Nb}$ face while it is along the maximum shear directions of 36–54° inclined to the interface when observed at the $(1\bar{1}0)$ face. The strain localization along a specific maximum shear direction results in the cleavage of Al_2O_3, always initiating from the interface possessing the $(110)_{Nb} \parallel (0001)_{Al_2O_3}$ and $[1\bar{1}0]_{Nb} \parallel [0\bar{1}\bar{1}0]_{Al_2O_3}$ orientation relationship.

Keywords HRTEM · ELNES · Nb/Al_2O_3 interfaces · Strain measurements

C. Scheu · Y. Liu · S. H. Oh · D. Brunner · M. Rühle
Max-Planck-Institut für Metallforschung, Heisenbergstr. 3, 70569 Stuttgart, Germany

C. Scheu (✉)
Department Physical Metallurgy and Materials Testing, Montanuniversität Leoben, Franz-Josef-Str. 18, 8700 Leoben, Austria
e-mail: christina.scheu@notes.unileoben.ac.at

Y. Liu
Institute for Physics & Centre for Micro- and Nanotechnology, Technische Universität Ilmenau, Ernst-Abbe-Zentrum, Ehrenbergstraße 29, Postfach 100565, 98684 Ilmenau, Germany

S. H. Oh
Erich Schmid Institut für Materialwissenschaft, Österreichische Akademie der Wissenschaften, Jahnstr. 12, 8700 Leoben, Austria

Introduction

The atomic and electronic structures of Nb/Al_2O_3 interfaces have been investigated in a large number of experimental and theoretical studies [1–16]. Reasons for these studies are that the system can be considered as a model metal–ceramic system since no reaction phases are expected to form even at elevated temperatures and thermal stresses can be neglected due to similar thermal expansion coefficients. In addition, a strong adhesion can be achieved, and atomically abrupt interfaces can be easily produced by molecular beam epitaxy (MBE), internal oxidation or solid-state diffusion bonding.

Experimental studies on thin Nb films deposited by MBE at 850 °C on (0001) Al_2O_3 single crystals showed the following orientation relationship (OR I): $(111)_{Nb} \parallel (0001)_{Al_2O_3}$ and $[101]_{Nb} \parallel [2\bar{1}\bar{1}0]_{Al_2O_3}$ [4, 6, 11, 17]. The OR is established due to an unique building principle where the Nb atoms try to occupy Al lattice sites of a continued Al lattice of the Al_2O_3.

High-resolution transmission electron microscopy (HRTEM) revealed that the interface is semi-coherent [4, 6, 11, 12]. In between the coherent regions misfit dislocations formed to compensate the lattice mismatch and they were found to be situated directly at the interface [11, 12]. Electron energy-loss near-edge structure (ELNES) studies performed on these samples indicated an oxygen terminated Nb/Al_2O_3 interface [7]. First-principle calculations using periodic boundary conditions and neglecting the misfit dislocations revealed that this termination leads to a low energy configuration [9, 13, 14]. However, total energy calculations performed by Batyrev et al. have indicated that the termination and thus the adhesion strongly depend on the oxygen partial pressure [16]. Vitek and co-workers have performed calculations for this $(111)Nb/(0001)Al_2O_3$ interface orientation using a simple pair-potential description for the Nb and Al_2O_3 interaction [8, 15]. The results showed that, depending on the bond strength, the misfit dislocation can be either located directly at the interface (as observed for the MBE samples) or possess a stand-off of about four lattice planes from the interface into the Nb lattice.

Nb/Al_2O_3 interfaces prepared by internal oxidation at 1500 °C revealed a different OR as the one of the MBE films, which is most likely caused by differences in the kinetics during the growth process. It was found that the following planes and directions are parallel to each other: $(110)_{Nb} \parallel (0001)_{Al_2O_3}$ and $[1\bar{1}0]_{Nb} \parallel [2\bar{1}\bar{1}0]_{Al_2O_3}$ (OR II) [2, 3, 18]. The interface is also semi-coherent, but in contrast to the MBE films, the misfit dislocations possess a stand-off of about four $(110)_{Nb}$ planes within the Nb lattice [2]. However, no information is available on the bonding mechanism established across the interface between the Al_2O_3 precipitates and the surrounding Nb matrix and in general a theoretical description of this interface orientation is missing. It is interesting to note that the $(111)Nb/(0001)Al_2O_3$ films, deposited by MBE at 850 °C, change their orientation relationship during annealing at 1500 °C to the one which is established during internal oxidation, i.e. $(110)Nb/(0001)Al_2O_3$ in order to lower the total energy [10].

Solid-state diffusion bonding experiments have been performed using a variety of different interface planes and orientations of the two crystals and mechanical tests were conducted on those samples as will be described below. The atomic and electronic structure has only been investigated for solid state diffusion bonded samples prepared at 1700 °C which possess OR II of the internal oxidized samples [5, 7]. No mechanical tests have been performed on these particular samples. The HRTEM investigations revealed again a semi-coherent interface, but the stand-off of the dislocation was only 2 to 3 $(110)_{Nb}$ planes within the Nb [5]. HRTEM image simulations indicated that the interfacial terminating plane is an Al layer with a density 1.5 times higher than the density of an double Al terminating layer [5]. The presence of Al atoms at the interface was also confirmed by ELNES studies [7].

As mentioned before, the mechanical properties of the Nb/Al_2O_3 system have been investigated exclusively at diffusion bonded joints using a variety of specimen geometries and methods [19–24]. The fracture properties of Nb/Al_2O_3 bicrystals were studied using four-point bending tests with single-edged notched beams [19–21]. It was found that the interfacial fracture energy depends strongly on the interface planes of Nb and Al_2O_3. For samples possessing the MBE orientation (OR I) the fracture energy is 112 ± 51 J/m^2. For those having the orientation of the internal oxidized samples (OR II) the value is much higher and amounts to 1899 ± 213 J/m^2. A similar high value of 1876 ± 610 J/m^2 was achieved for samples which had OR III with $(110)_{Nb} \parallel (0001)_{Al_2O_3}$ and $[1\bar{1}0]_{Nb} \parallel [01\bar{1}0]_{Al_2O_3}$. In general, higher fracture energies are related to a larger plastic deformation of the Nb as observed by slip lines on the Nb fracture surface [19–21]. Evaluation of the loading and fracture characteristics revealed that sharp precursor cracks developed initially in the Al_2O_3 [19–21]. Recent fracture toughness tests using chevron-notched bending bars, which were performed by Bartsch et al. on $Al_2O_3/Nb/Al_2O_3$ sandwiches possessing two different interface ORs (asymmetrical set-up), showed similar fracture characteristics to the ones observed in single-notch bending tests [24]. That is, a severe plastic deformation of the Nb and cracking in the Al_2O_3 [24]. Scanning electron microscopy (SEM) investigations of the fracture surfaces revealed that the cleavage occurs along pyramidal faces of the Al_2O_3 [24]. Compression test were carried out on $Al_2O_3/Nb/Al_2O_3$ sandwiches with different OR at the interface (but with a fixed OR within one sandwich) and different metal layer thicknesses [21–23]. The results indicate that with decreasing metal layer thickness the stress necessary to initiate a crack increases drastically while the interface orientation seems to have no significant effect [21–23].

In the present study, full-field optical strain measurements (FFOM) were applied to niobium crystal faces during compressive deformation of a sandwich-bonded $Al_2O_3/Nb/Al_2O_3$ joint possessing two different interface ORs. The diffusion bonded sample was the same one that was investigated in the work of Bartsch et al. [24], where we had performed fracture toughness test and SEM analysis of the fractures surfaces as

mentioned above. The aim of the present work was to study experimentally the development of strain and its variations within the single-crystalline Nb layer during compression and to determine how the strain is influenced by the interface orientation within the joint. To our best knowledge it is the first time that the FFOM method is used to investigate samples consisting of single-crystalline materials. The method has been successfully applied to polycrystalline Al_2O_3/Nb/Al_2O_3 couples allowing a detailed study of the development of strains [25, 26]. If the FFOM method is applicable to the chosen system, the plastic deformation and cracking at the metal–ceramic interfaces can be studied in-situ allowing to get further insight into the mechanical behaviour of such systems. Prior to the deformation tests, the initial interface structures of the Al_2O_3/Nb/Al_2O_3 sandwich were investigated in detail by various transmission electron microscopy (TEM) methods. The atomic structure was studied by HRTEM, which was performed in two perpendicular viewing directions. In addition, ELNES investigations have been conducted to determine experimentally the bonding that is established at the interfaces.

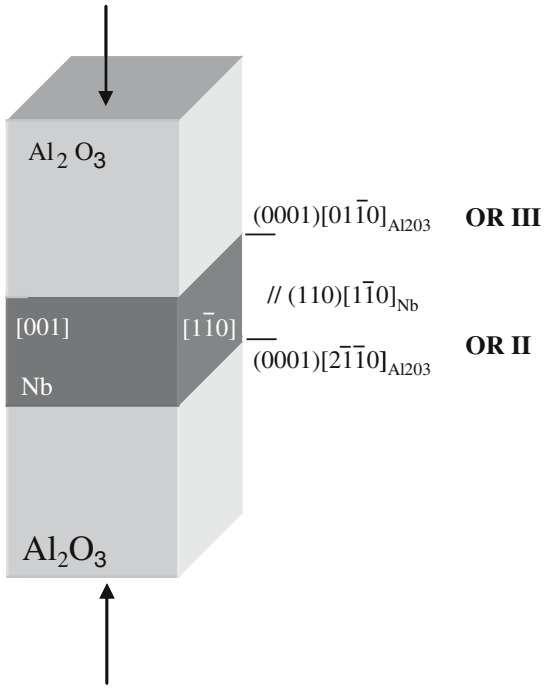

Fig. 1 Orientation relationships of the Al_2O_3/Nb/Al_2O_3 sandwich

Experimental

Material

The sandwich was prepared by solid state diffusion bonding which was performed in ultra-high vacuum (UHV) at nominally 1400 °C for 3 h using a load of 7 MPa. Details of the diffusion bonding apparatus are given elsewhere [27, 28]. The specimen consists of a 2 mm thick Nb single crystal joined to two 3 mm thick α-Al_2O_3 single crystal pieces. An asymmetrical set-up had been chosen where two different orientation relationships between the two α-Al_2O_3 single crystals and the one Nb single crystal exist. The following orientation relationships were used (Fig. 1):

OR II : $(110)_{Nb} \parallel (0001)_{Al_2O_3}$, $[1\bar{1}0]_{Nb} \parallel [2\bar{1}\bar{1}0]_{Al_2O_3}$,
which is equivalent to
$(110)_{Nb} \parallel (0001)_{Al_2O_3}$, $[001]_{Nb} \parallel [01\bar{1}0]_{Al_2O_3}$,

OR III: $(110)_{Nb} \parallel (0001)_{Al_2O_3}$, $[1\bar{1}0]_{Nb} \parallel [01\bar{1}0]_{Al_2O_3}$,
which is equivalent to
$(110)_{Nb} \parallel (0001)_{Al_2O_3}$, $[001]_{Nb} \parallel [2\bar{1}\bar{1}0]_{Al_2O_3}$.

The interfaces are characterized by the planes and directions in the Nb and α-Al_2O_3 lattices which are parallel to the interface plane. Prior to the diffusion bonding, the Al_2O_3 single crystals have been sputter-cleaned using 1 keV Ar^+ ions, followed by an annealing for 2 h at nominally 1000 °C in UHV.

Crystallography

For the (0001) basal plane orientation, the α-Al_2O_3 crystal is build up by an alternating stacking sequence of one oxygen and two aluminium layers. Three different bulk terminations of the (0001) α-Al_2O_3 surface are possible: single aluminium, double aluminium or oxygen termination [29]. Accordingly, different bonding mechanisms involving either Nb–O, Nb–Al or mixed bonds might occur at an atomically abrupt Nb/(0001)Al_2O_3 interface.

In the present study the α-Al_2O_3 lattice is taken as a reference lattice to calculate the lattice mismatch δ:

$$\delta = \frac{d_{Nb} - d_{Al_2O_3}}{d_{Al_2O_3}},$$

d_{Nb} and $d_{Al_2O_3}$ are the lattice plane spacings of Nb and Al_2O_3, respectively. For a hard sphere model without considering any relaxations at the interface, the spacing D between misfit dislocations is given by [5]:

$$D = \left| \frac{d_{Nb} \cdot d_{Al_2O_3}}{d_{Nb} - d_{Al_2O_3}} \right|.$$

Transmission electron microscopy

For the TEM investigations, cross-sectional TEM specimens were prepared following the technique described in [30]. For each interface two types of TEM specimens were made with the viewing direction in the electron microscope being parallel either to the $[001]_{Nb}$ or $[1\bar{1}0]_{Nb}$ direction. After ion milling, the specimens were carbon coated to avoid charging effects. The microstructure of the different Nb/Al_2O_3 interfaces was studied in detail by HRTEM using a JEOL JEM ARM1250 microscope with a point resolution of 0.12 nm at 1250 kV. Several HRTEM micrographs have been qualitatively analyzed for each specimen and viewing direction in order to obtain better statistics for e.g. distance between misfit dislocations. Analytical TEM was performed with a dedicated scanning TEM (VG HB 501 UX) operated at 100 kV. The microscope is equipped with a cold field emission electron gun, an ultra-thin window Si(Li) energy-dispersive X-ray spectrometer and with a parallel electron energy-loss spectrometer (EELS) (Gatan DigiPEELS 766 up-graded to a UHV Enfina system). The interface-specific components of the ELNES were obtained using the spatial difference technique [7, 31, 32] in order to investigate the bonding mechanism.

Mechanical test and strain measurements

The $Al_2O_3/Nb/Al_2O_3$ joints were deformed in compression tests using a Zwick deformation machine. The load was applied uni-directionally through the moving beam to the top end of the joint while the lower part was fixed. As a consequence of this setup, the motion in loading direction occurred mainly at the upper interface while that at the lower interface was small due to the negligible deformation of Al_2O_3. It is suspected that this difference in motion might generate asymmetrical deformation at the two interfaces. Therefore, we have also performed the tests by reversing the specimen orientation. The surface strains occurring at the Nb layer were measured with a FFOM set-up, which is described in detail in [25, 26]. It consists of the specimen, two CCD cameras arranged in such a way that images are taken at each load level of interest from two perpendicular faces of the sample, a normal light source for illumination, and a software which converts the information in the images into strain or displacement data [25, 26]. Prior to the deformation, a stochastic black–white contrast pattern was produced on two perpendicular niobium faces by first colouring these faces white followed by spraying a black lacquer on it. For the present investigation these surfaces are both the (001) and the $(1\bar{1}0)$ planes (Fig. 1). During deformation the stochastic pattern changes and by comparing these changes to reference images, e.g. the undeformed state, a full-field map of the strain or surface displacement at various deformation stages can be obtained [25, 26]. By using two cameras it is possible to determine the three-dimensional (3D) displacement and strain field.

For the joints investigated, the load is applied to the (0001) basal plane face of the single-crystalline Al_2O_3 parts as indicated in Fig. 1. During the compression tests the compressive load and the displacement of the cross-head are measured simultaneously by a linear variable displacement transducer (LVDT) and these data are used to calculate stress–strain curves.

The von Mises strain ϵ_m is used in presenting the strain maps from FFOM measurements which is given by the following equation:

$$\varepsilon_m = \frac{\sqrt{2}}{3}\left[(\varepsilon_1-\varepsilon_2)^2+(\varepsilon_2-\varepsilon_3)^2+(\varepsilon_3-\varepsilon_1)^2\right]^{\frac{1}{2}}. \quad (1)$$

ε_1, ε_2, ε_3 are the strains in the principal axes. The advantage of using the von Mises strain is that it is independent of the coordinate system [25, 26].

Results and discussion

Interface structure

Figure 2a displays a HRTEM micrograph of the $Nb/(0001)Al_2O_3$ interface with orientation relationship II. The image was taken in $[1\bar{1}0]_{Nb}$ zone axis and it shows that the interface is atomically abrupt. For this viewing direction the lattice mismatch of OR II amounts to $\delta_1 = +20.4\%$ and the corresponding distance between misfit dislocations should be $D_1 = 0.81$ nm. In the experimental image misfit dislocations are present on average every 0.82 nm to accommodate the lattice mismatch. Every fifth $(002)_{Nb}$ plane is ''missing'' with respect to the adjacent lattice planes of the Al_2O_3. This can be seen more clearly in an inclined view of the recorded lattice image (Fig. 2b), which was obtained by a simplified Scheimpflug technique [33]. The corresponding strain field is not strongly pronounced and only slightly visible in the Nb crystal adjacent to the interface. The misfit dislocations observed in $[001]_{Nb}$ zone axis of the same interface are additional $(\bar{1}10)_{Nb}$ planes which have in average a stand-off position of about two $(110)_{Nb}$ plane spacing. One misfit dislocation is marked in the HRTEM micrograph displayed in Fig. 2c. Coherent regions exist between the misfit

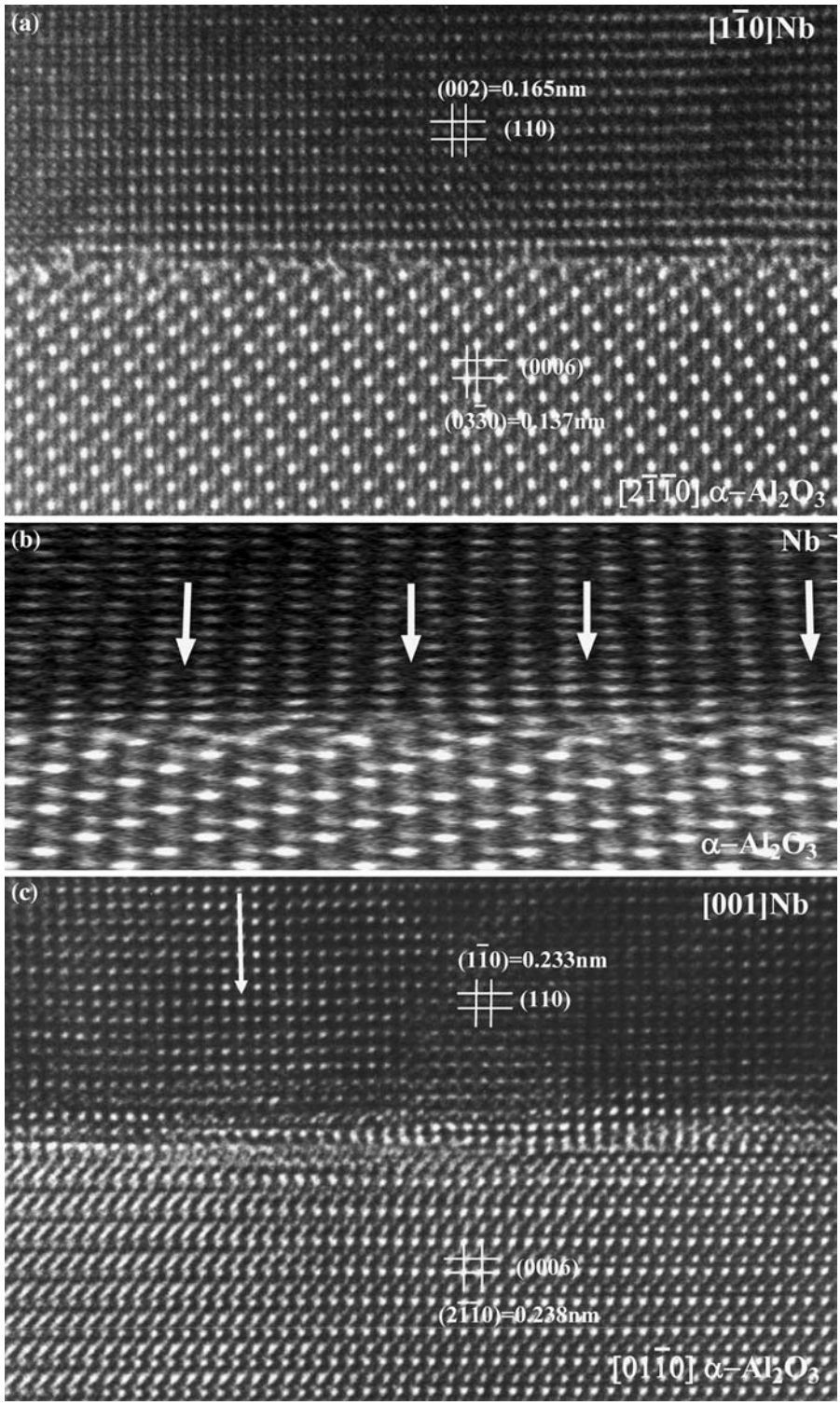

Fig. 2 HRTEM image of the atomically abrupt Nb/$(0001)Al_2O_3$ interface with OR II taken (**a**) in $[1\bar{1}0]_{Nb}$ and $[2\bar{1}\bar{1}0]_{Al_2O_3}$ zone axis and (**b**) a corresponding inclined projection view for better visibility of the missing Nb planes. (**c**) displays the lattice image in $[001]_{Nb}$ and $[01\bar{1}0]_{Al_2O_3}$ zone axis

dislocations. The average distance between the misfit dislocations is 11 nm which agrees with the theoretical value of 11.1 nm corresponding to the lattice mismatch of $\delta_2 = -2.1\%$. Again, some lattice bending is associated with the misfit dislocation cores. The observations for the two different directions that lattice planes are inserted or missing according to the lattice mismatch and that at least some weak lattice bending occurs, indicate that a semi-coherent interface has formed.

The HRTEM results obtained in $[001]_{Nb}$ zone axis are in agreement with observations of Knauss and Mader [5]. They have also studied a diffusion bonded

sample possessing OR II and found a similar same stand-off value for the misfit dislocations in $[001]_{Nb}$ zone axis. However, they did not detect a regular dislocation spacing of the misfit dislocation as it was observed in the present work. Knauss and Mader [5] explained this with the presence of Al_2O_3 surface steps which occurred with a non-regular distance and which act as nucleation sites for interfacial dislocations. The authors were also not able to detect any relaxations indicative for the presence of misfit dislocations in $[1\bar{1}0]_{Nb}$ zone axis, since they used a TEM with a point-to-point resolution of 0.17 nm. So they could not resolve the $(03\bar{3}0)_{Al_2O_3}$ planes with a spacing of 0.137 nm which are perpendicular to the interface plane. These planes are marked in Fig. 2a and were used together with the $(002)_{Nb}$ planes to calculate the lattice mismatch $\delta_1 = +20.4\%$.

The Nb/$(0001)Al_2O_3$ interface with orientation relationship III was not studied yet by HRTEM. Figure 3a shows a lattice image of this interface taken in $[1\bar{1}0]_{Nb}$ zone axis. Again, no extended reaction layer is visible and the interface is atomically abrupt. On average every 0.55 nm a $(002)_{Nb}$ plane is inserted in the Nb lattice which is in accordance to the lattice mismatch of $\delta_3 = -30.7\%$ (Fig. 3a, b). As observed for the interface possessing OR II, a bending of the $(002)_{Nb}$ planes in the vicinity of the inserted planes is not strongly pronounced and difficult to detect even when viewed under an inclined angle (Fig. 3b). The HRTEM micrograph of this interface in $[001]_{Nb}$ zone axis is displayed in Fig. 3c. In average every sixth to seventh $(\bar{1}10)_{Nb}$ plane coincides with every seventh to eight $(02\bar{2}0)_{Al_2O_3}$ plane. This is in agreement with the corresponding lattice mismatch of $\delta_4 = 13.6\%$ for this direction. The interface is again semi-coherent and exemplary two misfit dislocations are indicated by arrows in Fig. 3c.

The HRTEM investigations (Figs. 2, 3) reveal that both interfaces are atomically abrupt and that no extended interfacial reaction phases have formed. This is in accordance to thermodynamical data [34, 35] which predict that only dissolution of Al and O in Nb is possible without any reaction phase formation at the present bonding conditions. In addition, no impurities were detected by EDS measurements at the interfaces or within the Nb and Al_2O_3 single crystals. The bonding behaviour at the atomically abrupt interfaces was studied by ELNES investigations. The results indicated that, independent of the interface orientation, the Al atoms are involved in the interfacial bonding. Figure 4 shows as an example the interfacial Al-$L_{2,3}$-ELNES determined at the interface possessing OR III. The threshold occurs at 77 eV and two broad peaks appear at around 86 eV and 98 eV. No other prominent features, such as the strong peak at 79 eV characteristic for bulk α-Al_2O_3, occur in the interfacial ELNES (Fig. 4). The obtained interfacial spectrum can be attributed mainly to a change in the local Al coordination, which is only possible if the Al atoms are located directly at the interface, i.e. the Al_2O_3 substrate is Al-terminated. Similar observations were made for the interface having OR II. The results are in accordance to the studies of Bruley et al. [7], who found the same bonding behaviour at diffusion bonded Nb/Al_2O_3 samples possessing OR II. In contrast, an O-terminated interface configuration was detected by Bruley et al. at the interface between thin MBE grown (111) Nb films on (0001) Al_2O_3 substrates [7]. The difference in the bonding behaviour is most likely due to the different Al_2O_3 substrate treatment procedures. Recent studies on Cu/$(0001)Al_2O_3$ interfaces have shown that the cleaning procedure prior to the thin film deposition or the diffusion bonding process is crucial for the Al_2O_3 surface termination and thus for the bonding behaviour [36, 37].

Strain development under compression

The strain development under compression was studied at the identical sandwiches which had been investigated by HRTEM and ELNES analysis. The stress–strain curves of the specimen obtained by FFOM and LVDT measurements are displayed in Fig. 5. Thereby, an average strain of the $(1\ \bar{1}0)$ and (001) faces was used for the FFOM data. The stress values calculated from FFOM are always higher than the values obtained by LVDT due to the smaller strain measured by FFOM. This was also found for polycrystalline Al_2O_3/Nb/Al_2O_3 diffusion bonded joints [25, 26]. The fracture stress is about 90 MPa and thus much lower than the fracture stress of polycrystalline joints which have fracture stresses exceeding 300 MPa [25, 26]. However, the obtained data are in good agreement with measurements performed by Soyez et al. [21–23] on single-crystalline, diffusion bonded Al_2O_3/Nb/Al_2O_3 joints. They had used several orientation relationships between the Al_2O_3 and the Nb, but always symmetrical set-ups (only one orientation relationship between the two Al_2O_3 single crystals and the single-crystalline Nb layer) and found a strong dependence of the fracture stress on the Nb thickness [21–23]. For the orientation relationship $(110)_{Nb} \parallel (0001)_{Al_2O_3}$, $[1\bar{1}0]_{Nb} \parallel [01\bar{1}0]_{Al_2O_3}$ (OR III in the present study, see Fig. 1) they found fracture stresses of about 200 MPa for a Nb thickness of 1.68 mm and 100 MPa for a thickness of 2.75 mm. Taking into account that our sandwich specimen has an

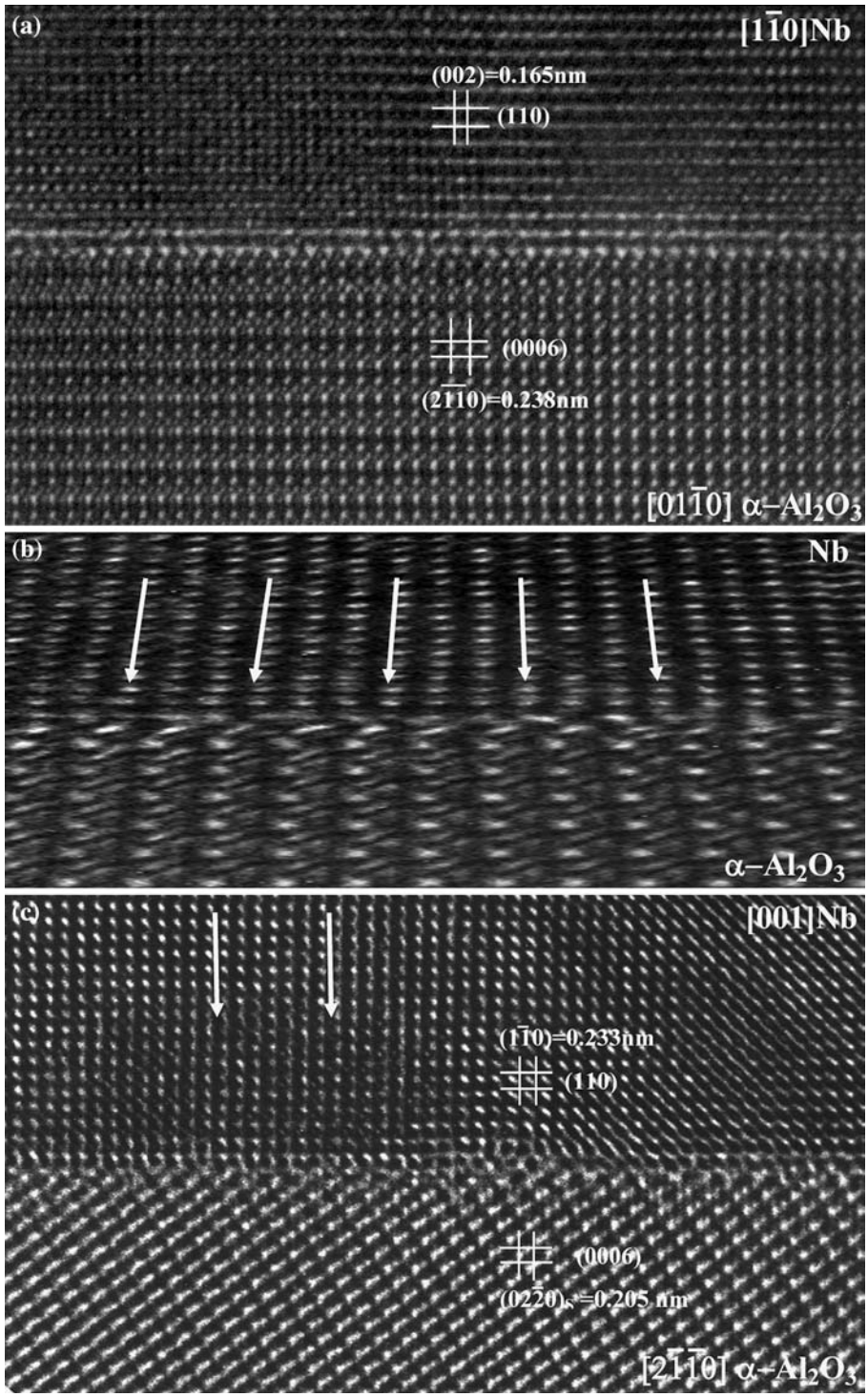

Fig. 3 HRTEM micrograph of the Nb/(0001)Al_2O_3 interface possessing OR III acquired (**a**) in $[1\bar{1}0]_{Nb}$ and $[01\bar{1}0]_{Al_2O_3}$ zone axis, and (**c**) in $[001]_{Nb}$ and $[2\bar{1}\bar{1}0]_{Al_2O_3}$ zone axis. (**b**) shows a inclined projection view of (**a**)

asymmetrical set-up and a different thickness, and that the data were obtained in the present study by FFOM measurements, our results are in good agreement with those of Soyez et al. [21–23].

The stress–strain curves in Fig. 5 exhibit first a linear-elastic regime followed by a transition to a plastic regime until fracture occurs as marked by "×" in the figure. Excluding any deformation in the Al_2O_3, we conclude that the niobium starts to deform elastically, then begins to yield (above 35 MPa) and finally fracture occurs in the Al_2O_3 single crystal. Figure 6 shows the strain maps received from different crystal faces of

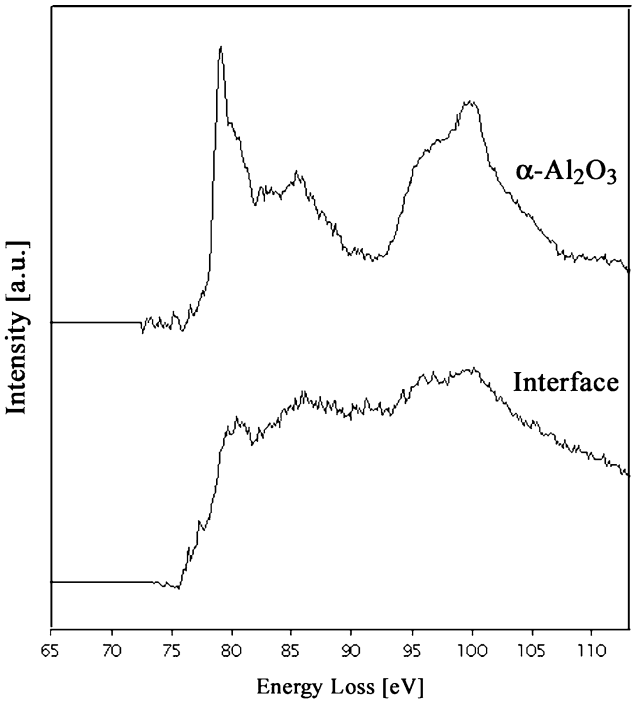

Fig. 4 Al-$L_{2,3}$-ELNES of bulk Al_2O_3 and from the Nb/(0001)Al_2O_3 interface possessing OR III. The interfacial signal was determined by the spatial difference technique

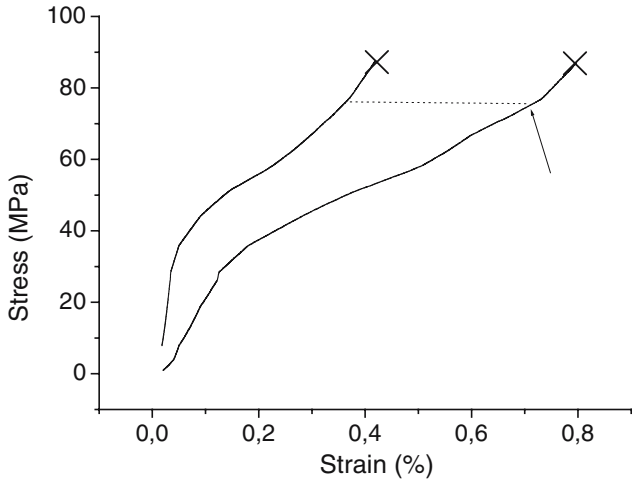

Fig. 5 Stress–strain curves obtained by full-field optical strain measurements (FFOM) and linear variable displacement transducer (LDVT) measurements. The dotted line corresponds to the strain maps shown in Fig. 6. The ''×'' indicates the fracture of Al_2O_3

the Nb layer after deformation to a compressive stress of 75 MPa. This point is indicated in the stress–strain curves displayed in Fig. 5. The arrows in Fig. 6 point to the positions of the interfaces. The colours in the figure always represent the intensity of the strain according to the attached scaling bar. The comparison between Fig. 6a and b shows that the strain localization pattern depends strongly on the respective crystal face of the Nb crystal. For the (001) face, the strain is highly localized at the Nb/Al_2O_3 interfaces with the values being slightly higher at the interface possessing OR III compared to the one having OR II (Fig. 6a). In contrast to the observations of the (001) plane, the strain is highest for the $(1\bar{1}0)$ plane in directions which are inclined to the interface plane at 36–54° starting from the four corners of the two interface planes (Fig. 6b). For the interface having OR III, additionally a high strain concentration occurs at the centre of the interface plane, which is continued in directions possessing an inclination angle of 45° relative to the interface (Fig. 6b). It seems that mainly slip systems of the type $\{112\}\langle 111\rangle$ and $\{110\}\langle 111\rangle$ are activated, which are the main slip systems for high purity Nb single-crystals at room temperature [38].

The results indicate that the strain localization depends on the interface orientation which is obviously at the $(1\bar{1}0)$ face, where differences in distribution of the high strain concentration regions were found for OR II and OR III. To check whether this phenomenon is not related to the loading direction of the asymmetrical crystal set-up, a second experiment was performed with the orientation of the sandwich reversed (interface with OR III at the lower part). Indeed, similar strain patterns were observed for both faces, even though the absolute values might be different as for example visible at the (100) face displayed in Fig. 6a, c. However, more importantly the differences in the strain localization for OR II and OR III as observed from the $(1\bar{1}0)$ face (Fig. 6b, d) are the same and thus independent of the loading direction. In both experiments, high strain concentrations are found at a middle point of the OR III interface and along directions inclined by 45° to the interface starting from this point, which are not pronounced at the OR II interface. It is this strain concentration, which leads to the fracture of sapphire displayed in Fig. 7. In conclusion, the results obtained by reversing the specimen orientation show that the experiments are indeed independent of the loading direction.

During further proceeding of the compression test, fracture of the Al_2O_3 was observed. Figure 7 shows the strain map acquired immediately after the fracture of the lower Al_2O_3 part at a compressive stress of 90 MPa. The fracture starts at the Nb/Al_2O_3 interface with OR III (same loading direction as in Fig. 6c, d) and proceeded into the Al_2O_3 single crystal. The fracture in the Al_2O_3 always started at the interface plane with OR III. Nevertheless, since both interfaces possess a strong adhesion, cracking does not occur directly at the interface and thus is not influenced by the

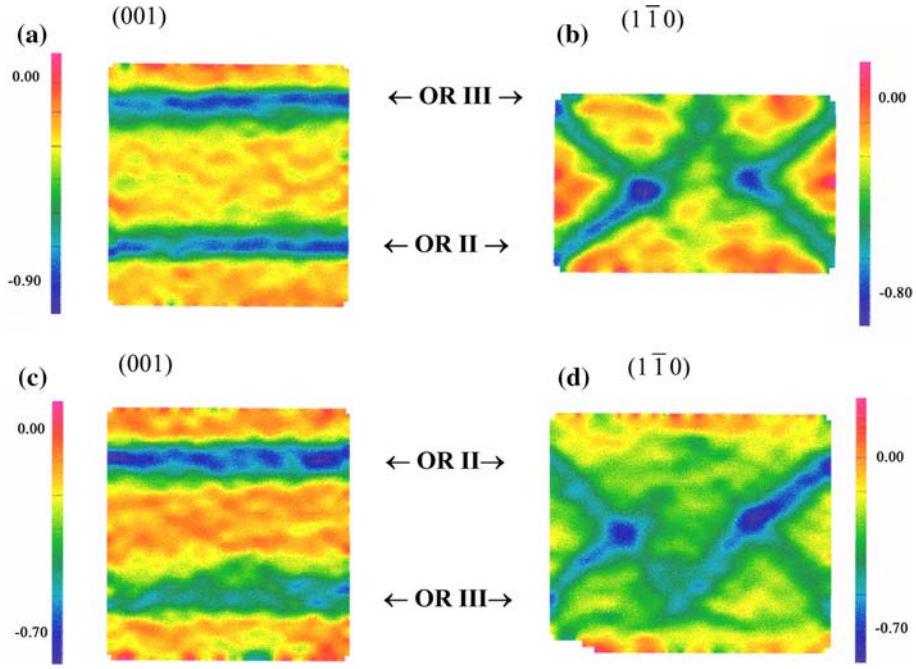

Fig. 6 3D cumulative von Mises strain maps taken at the (001) and (1$\bar{1}$0) planes of Nb, respectively. (**a**) and (**b**) were measured with the stacking sequence OR III/OR II (from top to bottom), and (**c**) and (**d**) were taken with the reversed stacking OR II/OR III

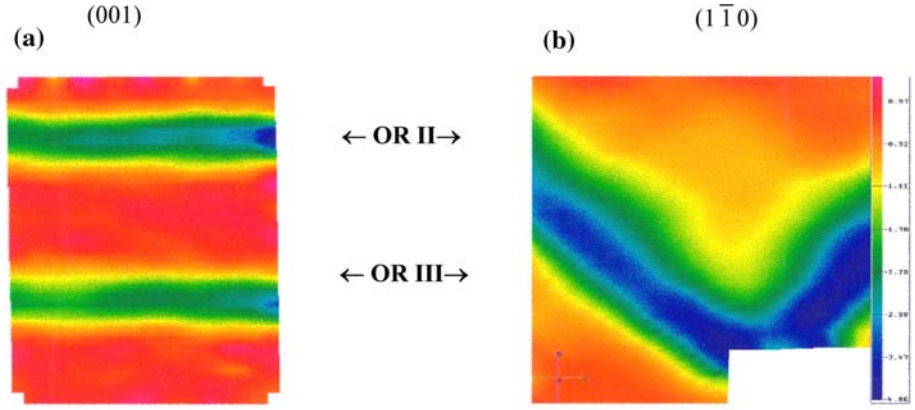

Fig. 7 3D cumulative von Mises strain maps measured at the (**a**) (001) and (**b**) (1$\bar{1}$0) plane of Nb during the fracture of Al_2O_3. The sandwiches had the stacking sequence OR II/OR III

in-plane interface orientation which is in accordance to the results of Soyez et al. [21–23]. Instead it is related to the geometrical orientation of the Al_2O_3 single crystal which allows an ''easier'' cleavage for OR III than for OR II. As reported by Bartsch et al. the measured fracture toughness values of the samples are in the order of 7 $MPam^{1/2}$ and thus similar to literature values for cleavage along the pyramidal faces [24]. As mentioned above this fracture characteristics was confirmed by SEM investigations of the fracture surfaces [24].

Our FFOM measurements confirm that the crack in the Al_2O_3 is initiated by strain concentration that is closely related with the pile-up of dislocations at the Nb/Al_2O_3 interface. This is in agreement with the results of Soyez et al. [21–23] and Bartsch et al. [24]. However, in contrast to those methods the FFOM technique allows to study directly the process by imaging the development of the strain in the Nb crystal during deformation. The crack formation itself can be explained by the modified Cottrell model developed by Soyez et al. [23].

Summary and conclusion

HRTEM studies performed at $Al_2O_3/Nb/Al_2O_3$ sandwiches with an asymmetrical set-up (OR II and OR III) revealed that semi-coherent interfaces have formed. Coherent regions are separated by misfit dislocations which compensate the lattice mismatch. For both interface orientations, Al–Nb bonds are established at the atomically abrupt interfaces as determined by ELNES investigations. FFOM measurements

were successfully applied to the identical sandwiches to measure the local strain during compression tests. The measurements enabled us to correlate the macroscopic mechanical behaviour represented by stress–strain curves with the FFOM strain maps with a resolution down to the mesoscale. The strain patterns at the two investigated Nb planes are different from each other. For the $(001)_{Nb}$ plane we found that the strain is localized at the interfaces. In contrast, the investigations on the $(1\ \bar{1}0)_{Nb}$ plane indicated that high strain levels occur for this plane along the maximum shear directions which are 36–54° inclined to the interface and start from the four corners of the interface planes. For the interface possessing OR III high strain concentrations are also found at a middle point of the interface and along maximum shear directions, which are inclined by 45° to the interface starting from the middle point. This strain localization finally leads to cleavage and thus to fracture within the Al_2O_3 single crystals. It is always the Al_2O_3 crystals next to the interface possessing OR III which breaks.

Acknowledgements Financial support by the Deutsche Forschungsgemeinschaft (DFG) is gratefully acknowledged. The authors wish to thank M. Bartsch and U. Messerschmidt for a fruitful cooperation within the DFG project and F. Ernst for his contribution to the project application. Helpful discussions with R. Cannon are acknowledged. The authors thank W. Kurtz for the diffusion bonding of the specimen and U. Salzberger for the TEM specimen preparation. The authors also wish to thank G. Dehm for careful reading of the manuscript.

References

1. Burger K, Mader W, Rühle M (1987) Ultramicroscopy 22:1
2. Mader W (1989) Z Metallkde 80(3):139
3. Mayer J, Mader W, Knauss D, Ernst F, Rühle M (1990) Mat Res Soc Symp Proc 183:55
4. Mayer J, Flynn CP, Rühle M (1990) Ultramicroscopy 33:51
5. Knauss D, Mader W (1991) Ultramicroscopy 37:247
6. Mayer J, Gutekunst G, Möbus G, Dura JA, Flynn CP, Rühle M (1992) Acta Metall Mater 40:S217
7. Bruley J, Brydson R, Müllejans H, Mayer J, Gutekunst G, Mader W, Knauss D, Rühle M (1994) J Mater Res 9(10):2574
8. Vitek V, Gutekunst G, Mayer J, Rühle M (1995) Phil Mag A 71(6):1219
9. Kruse C, Finnis MW, Lin JS, Payne MC, Milman VY, De Vita A, Gillan MJ (1996) Phil Mag Lett 73:733
10. Wagner T, Lorenz M, Rühle M (1996) J Mater Res 11(5):1255
11. Gutekunst G, Mayer J, Rühle M (1997) Phil Mag A 75(5):1329
12. Gutekunst G, Mayer J, Vitek V, Rühle M (1997) Phil Mag A 75(5):1357
13. Finnis MW (1998) Phys Stat Sol A 166:397
14. Verdozzi C, Jennison DR, Schultz PA, Sears MP (1999) Phys Rev Lett 82:799
15. Levay A, Möbus G, Vitek V, Rühle M, Tichy G (1999) Acta Mater 47(15):4143
16. Batyrev I, Alavi A, Finnis M (2000) Phy Rev B 62(7):4698
17. Durbin SM, Cunningham JE, Mochel ME, Flynn CP (1981) J Phys F 11:L223
18. Mader W (1987) Mat Res Soc Symp Proc 82:403
19. Korn D, Elssner G, Cannon RM, Rühle M (2002) Acta Mater 50:3881
20. Cannon RM, Korn D, Elssner G, Rühle M (2002) Acta Mater 50:3903
21. Soyez G (1996) PhD Thesis, University of Stuttgart
22. Soyez G, Elssner G, Rühle M, Raj R (1998) Acta Mater 46(10):3571
23. Soyez G, Elssner G, Rühle M, Raj R (2000) J Mater Sci 35:1087
24. Bartsch M, Zhang Z-F, Scheu C, Rühle M, Messerschmidt U (2004) Z Metallkde 95(9):779
25. Liu Y, Brunner D (2002) Z Metallkde 93(5):444
26. Liu Y, Kohnle C, Brunner D, Rühle M (2003) Z Metallkde 94(6):694
27. Korn D, Elssner G, Fischmeister HF, Rühle M (1992) Acta Metall Mater 40:S355
28. Kurtz W (2002) Z Metallkde 93(5):432
29. Batyrev I, Alavi A, Finnis M (1999) Faraday Discuss 114:33
30. Strecker A, Salzberger U, Mayer J (1993) Prakt Metallogr 30:482
31. Müllejans H, Bruley J (1995) J Microscopy 180:12
32. Scheu C (2002) J Microscopy 205:52
33. Bitzek L, Wunderlich WE, Mader W (1988) Prakt Met 25:384
34. Burger K, Rühle M (1989) Ultramicroscopy 29:88
35. Saiz E, Tomsia AP, Cannon RM (1998) In: Tomsia AP, Glaeser AM (eds) Ceramic microstructures: control at the atomic level, Plenum Press
36. Gao M, Scheu C, Wagner T, Kurtz W, Rühle M (2002) Z Metallkde 93(5):438
37. Scheu C (2004) Interface Sci 12(1):127
38. Duesbery MS, Foxall RA (1969) Phil Mag 20:719